

CFD SIMULATION OF A COUGHING DROPLET DIFFUSION IN THE ACCELERATING-MOTION METRO CABIN

Fang Liu^{1,2,3*}, Ge Peng^{1,2}

¹ School of Geomatics and Urban Information, Beijing University of Civil Engineering and Architecture, 102616 Beijing, China - LF@bucea.edu.cn, lfucea@gmail.com (F. Liu), 2108160121008@stu.bucea.cn (G. Peng)

² Key laboratory of Modern Urban Surveying and Mapping, National Administration of Surveying, Mapping and Geoinformation, 102616 Beijing, China

³ University of Wisconsin-Milwaukee, Milwaukee, 53211 WI, U.S.

Commission IV, WG IV/8 – GeoComputation and GeoSimulation

KEY WORDS: the modified RANS $k - \epsilon$ turbulence model; inertial effects on background flow; droplet diffusion; subway cabin; with varying acceleration motion state; CFD simulation.

ABSTRACTS: The metro cabin provides an effective way for the spread of the pneumonia virus when provides convenience to human beings. The cabin undergoes a series of motions of acceleration speed, uniform speed, and deceleration speed during the one-station travelling process. The induced flow of the accelerated moving cabin is the determinant of the air drag force on the cough droplets, and effect on the time-frequency characteristics and motion trajectories of droplets of different sizes. In this study, we established a momentum equation on droplets, affected by the inertial force correction term in the non-inertial frame. Then added the drag force from the velocity difference between the cough droplets and the background airflow, and simulated configurations as: 1) droplet spreading aerodynamic process from different face orientations of infected dummy, 2) six groups of size particles, and 3) variable speed motion phases. The numerical simulation provides a physical analysis idea for studying the relationship between the two-phase flow under the action of inertial force. This design of a ventilation environment in public transportation helps to reach a more profound understanding of the inertial precipitation mechanism of droplet jets.

1. INTRODUCTION

As a high-efficient traffic, the subway provides the convenience for people's transmission; however, it can exert a rapid spreading of the pneumonia virus among large-scale populations in close proximity, and thus threatening the human health (Hamidi and Hamidi, 2021). During one-station traveling, the metro cabin successively accelerates, moves at a constant speed, and decelerates. Considering the background flow interior of the metro cabin change relative velocity direction and magnitude during various motion phases, Talaei et al. (2019) has measured the flow. We guess the spread trajectory of the pathogenic droplet jets has been promoted or delayed by the induced airflow mentioned. Besides, the inertia force on the sneeze droplets will change the motion trajectory of droplets of different sizes, we try to get information on the infection probability. According to the Toronto Transit Commission (TTC) report, the epidemic showed a significant turning-down trend in early March, meanwhile, ridership dropped by 71% between March 8 and March 31 (Palm et al., 2021; Doucet et al., 2021). Harris (2020) empirically found that residents in New York zip code communities along both sides of the subway line had more confirmed cases than residents in zip code communities without the subway, especially in the first two or three months. The public transit network and modes are also becoming potential important catalysts for the virus to spread, may greatly accelerate the spread of infectious diseases, and increase the intensity of disease outbreaks in megacities (Mo et al., 2021). Under the background of upgrading of an epidemic, as well as the genetic variants as Delta and Omicron, the Covid-19 vaccines method and keep-safe-social-distance method could not defend the virus infection and transmission. It is really a tough task to defeat the virus permanently and completely.

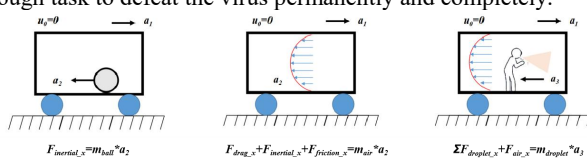


Figure 1. Research introduction: (a) a rigid ball motion in the accelerating cabin, (b) the airflow motion in the accelerating cabin, and (c) the drag force effect and the inertial force effect on the droplets.

The pathogen agents that droplets wrap up are the main sources of long-distance air-borne transmission, by coughing and sneezing. During short several seconds, the droplets clouds will propel and spread up to eight meters away by the high-momentum turbulent. The initial speed of sneezing will be up to 320 km/h, while that of cough will be up to 200-400 km/h; even the ordinary quiet talking, the number of droplets will be 500 (Bourouiba et al., 2014; Wang and Bourouiba, 2017). According to the record of (Flügge, 1978), large particle size droplets rapidly settle to the surface of attachments under the action of gravity, while small particle size droplets evaporate in the air, leaving the droplet core composed of protein and pathogens, which floats in the air for a long time in the form of an aerosol, and then contacts the human mucosa. In the metro cabin, the background wind produced by the relative movement between wall and flow will push back or forward the droplets towards the outlet during the acceleration and deceleration stages (Bourouiba, 2021).

At present, a large number of studies focused on the diffusion of cough droplets in a static indoor environment (Zeng et al., 2018; Richmond et al., 2011). Studies on transport characteristics of saliva droplets in a calm indoor environment, showed that the transport properties of cough-induced saliva droplets varied with sizes and different ventilation strategies (Aliabadi and Rogak, 2011; Cao et al., 2022). The application scenarios vary from offices to inpatient rooms. Zhong et al. (2019) studied the transport characteristics of saliva droplets produced by coughing in a calm indoor environment. He et al. (2011) studied the exhaled droplet transmission between occupants under different ventilation strategies in a typical office room. Yau et al. (2011) studied the transport and removal of respiratory droplets in the hospital ward environments.

Furthermore, there are also relevant studies on the uniform speed linear movement, including the outdoor

environment (Blocken et al., 2020) and the indoor environment (Wang et al., 2020). Blocken et al. (2020) study investigates whether a 1.5 m distance is a safe distance for two running persons. Wang et al. (2020) studied the increasing risk of contamination (defined as particle system entropy) in the whole room caused by one moving inpatient. However, studies on cough droplets subjected to inertial forces under the dynamic acceleration process are rare (Sun et al., 2020). These researches can refer to the electrostatic field (Matsuo et al., 2011) or the accelerating trains (Li, 2014). In terms of engineering experiments, Talaei et al. (2019) has measured and analyzed the background flow interior of the metro cabin, however, the role of it to the transmission of pathogens has not been dug furthermore.

Moreover, in non-inertial frame, the inertial force on the droplets during the acceleration or deceleration stages is non-negligible. Although droplets are paltry, they are widely affected by the air drag force, gravity, buoyancy, and other forces (Brownian force, surface tension, thermophoresis force, mass additional force, pressure gradient force, basset force, Magnus lift, Saffman lift) (Said et al., 2021). In general, the diameters of cough droplets are wide range, typically from 0.1-1000 μm . Although small droplets contain fewer virions, these can remain airborne for prolonged periods and thus cause "long-distance transmission" (Li et al., 2022). Hence we picked six typical diameters 3.5 μm , 6 μm , 20 μm , 50 μm , 112 μm , 175 μm , to describe the movement of the particle phase in practical problems.

On the basis of previous research, this study used 3D modeling and computational fluid dynamics (CFD) software to simulate the background inflow in the metro cabin and the motion trajectories of different-size droplets, including various motion states and three facing orientations. So with the push of background flow, it will promote the diffusion of the pollution droplet further or opposite direction. Therefore, it is reasonable to judge whether a fixed social distance in a non-inertial frame of reference is a safe method. It is very important to study the spray distance of droplet droplets in the state of variable acceleration in the cabin.

2. THEORY AND MODELS

2.1 Governing functions and numerical model

In order to simulate the induced wind circumstances in the cabin and the dispersion of droplets with the impact of it, during the acceleration, deceleration, and uniform speed phases, we used the Sketchup 3D modelling software and Ansys Fluent simulation software.

The inner wall of the cabin is set as the no-slip boundary condition, and the transient problem with time-varying boundary conditions was derived using the method of separation of variables, the reference superposition principle, and the Duhamel integral. Using the modified RANS (Reynolds-Average Navier-Stokes) $k-\epsilon$ turbulence model (with inertial force correction term), the particle momentum equation of cough droplets through airflow is established, and we use the Lagrangian particle tracking method to track the trajectory of cough particles.

Firstly, the mean velocity value distributes different spatially, and the airflow velocity distribution is expressed as (Talaei et al., 2019):

$$\left(\frac{\partial^2 w_s}{\partial x^2} + \frac{\partial^2 w_s}{\partial y^2}\right) = 0 \quad (1-a)$$

$$w_s(0, y) = w_s(L, y) = a \quad (1-b)$$

$$w_s(x, 0) = w_s(x, H) = a \quad (1-c)$$

Secondly, the transient velocity value with time-varying boundary conditions is constructed. In the analytical method, the steady-state equation and boundary conditions under inhomogeneous boundary conditions are expressed as below:

$$\frac{\mu}{\rho} \left(\frac{\partial^2 w_t}{\partial x^2} + \frac{\partial^2 w_t}{\partial y^2} \right) = \frac{\partial w_t}{\partial t} \quad (2-a)$$

$$w_t(0, y, t) = w_t(L, y, t) = 0 \quad (2-b)$$

$$w_t(x, 0, t) = w_t(x, H, t) = 0 \quad (2-c)$$

Merge the above two parts we could get the real-time solution:

$$w_g = w_s + w_t \quad (3-a)$$

Using the Duhamel integral rule and the separation variable method, we could calculate the analytical solutions to transient problems:

$$w_g(x, y, t) = at + \frac{16a}{\pi^2} \sum_{m=1}^{\infty} \sum_{n=1}^{\infty} \sin^2\left(\frac{n\pi}{2}\right) \sin^2\left(\frac{m\pi}{2}\right) \sin\left(\frac{n\pi}{L}x\right) \sin\left(\frac{m\pi}{H}y\right) \cdot \left[\frac{1}{\rho} \left(e^{-\frac{\mu k_{mn}^2}{\rho}} - 1 \right) \right] \quad (3-b)$$

The above expression is the analytical solution of the absolute velocity of flow considering the acceleration motion of the cabin, that is, the cabin induced flow (or called the interior background flow).

The finite volume method was employed to solve the continuity and momentum equations using the CFD package ANSYS Fluent 21.0. In the stationary metro cabin (or in a straight line in a uniform speed phase), the cabin itself is in the inertial reference frame. In this frame, the human body is assumed to be at the same speed as the metro's movement (with the seat belt on), and the cough is ejected in the form of a jet. Assuming that the droplet is a sphere centered on the pathogen and does not deform, and the specific forces are: the drag force, the gravity, the buoyancy, and the lift force. Other forces (thermophoresis force, virtual mass force, pressure gradient force, Brownian force et al.) can be ignored.

Furthermore, in an inertial reference frame, the force balance equations of the moving droplets are expressed as Eq (4-a). However, the mesh should be dynamic along with time. This is complex. Hence, the cabin is assumed to be fixed, and the velocity of interior induced flow is varying-time. in the non-inertial frame, a source term of momentum equation is added in Eq. (4-b).

The inertial frame (based on the fixed ground):

$$m_p \frac{d\vec{u}_p}{dt} = m_p \frac{\vec{u}_p - \vec{u}_g}{\tau} + m_p \frac{\vec{g}(\rho_p - \rho_g)}{\rho_p} + F_L \quad (4-a)$$

The non-inertial frame (based on the accelerating cabin):

$$m_p \frac{d(\vec{u}_p - \vec{u}_0)}{dt} = m_p \frac{\vec{u}_p - \vec{u}_g}{\tau} + m_p \frac{\vec{g}(\rho_p - \rho_g)}{\rho_p} + F_L + F_x \quad (4-b)$$

where, m_p [kg] is the constant mass of one droplet, \vec{a}_0 is the acceleration speed of the moving cabin, \vec{u}_g , \vec{u}_p , \vec{u}_0 [m/s] is the velocity of airflow, one droplet, and the cabin, ρ_g , ρ_p [kg/m³] is the density of airflow and water, τ is droplet relaxation time, and F_L [kg*m/s²] is the Saffman lift force acting on it. The term $m_p \frac{\vec{u}_p - \vec{u}_g}{\tau}$ is the resistance per unit particle mass, the

term $m_p \frac{\vec{g}(\rho_p - \rho_g)}{\rho_p}$ is the resultant force of particle gravity and

buoyancy, and the term $m_p \frac{d(\vec{u}_p - \vec{u}_0)}{dt}$ is the acceleration of particles relative to the cabin per unit particle mass.

Here, what needs to be paid attention to are the relative motion direction of airflow to the cabin, the face orientation, and the direction of the initial velocity of the droplet jet during various stages. The drag force affecting the particle motion is caused by the velocity difference between the fluid relative to the cabin. For instance, when the cabin is in the acceleration phase, the relative movement direction of the airflow and the cabin is opposite, and the flow is directed towards the outlet. Vice versa, in the deceleration phase, the two directions are the same and flow is toward the inlet. For droplets, the direction of the resistance is opposite to the direction of the droplet motion trajectory, and the direction of the inertial force on droplets is opposite to the direction of the cabin motion.

The DPM source terms model is well documented in the ANSYS Fluent theory guide. Then we update the "UDF-source" in the "Discrete Phase Model" with the linear acceleration rate of "Mass*0.9 [m/(s^2)]", where $F_x = m_p \vec{a}_0$ is an additional acceleration (force/unit particle mass) term. The time-varying interior the flow velocity was updated relative to the moving cabin. The function "Vel" was constructed using the "Named Expressions" model. The turbulent dispersion of droplets is tracked by stochastic tracking with the discrete random walk (DRW) model, enabling instantaneous turbulent fluctuations on the droplet trajectories. The DRW 27 Two-way turbulence coupling is used in numerical modeling to allow the effect of damping or turbulent eddies produced by droplets, which contributes to turbulent kinetic energy production.

2.2 Geometry, wind profile, and meshing settings

The geometry of the cabin is referring to the measurement of (Talaee et al., 2019). In Fig. 1, one cabin section unit with a pair of inlet and outlet connections is established as one solid model. In our study, the 3D model of the human body is represented by a 1.73 m (height) * 0.3 m (thickness) * 0.4 m (width) dummy, which is the same as the work of Yan et al.(2020).

Considering the viscosity and the temperature disparity, the spatial distribution of flow is various. According to the boundary layer theory (Oleinik and Samokhin, 2018), the mean velocity profile is approximate as

$$\bar{U} = 0.99U_\infty, \quad (5)$$

where, \bar{U} , called the free stream velocity, is the velocity at some distance above the boundary reaching a constant value. Meanwhile, the time-dependent velocity is measured in the inlet connection without mechanical ventilation. The specific measurements are complicated to refer to Talaee et al. (2019).

Put the processed cabin geometry into the Fluent Meshing model for mesh. Therefore, we get 1157895 poly-hexcore grids.

Add the dummy model, and perform mesh refinement to get the more delicate grids. It should be noted that the mannequin is designed to cover its mouth with the left hand close to the face, and the left hand is 12 cm away from the nozzle, which is the same as the behavior of people when coughing and sneezing. Draw a circular spout (particle injection surface) with a diameter of 2cm at the mouth position. By adding 3 layers of boundary layers near the human body, and finally the total number of grids including the cabin and the human body is 2899020.

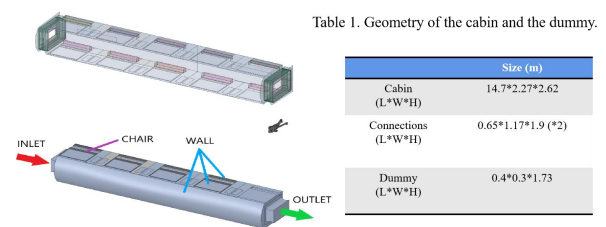
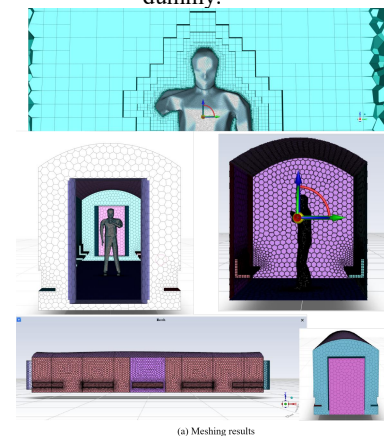


Figure 2. The geometry of the vacant cabin and the dummy.



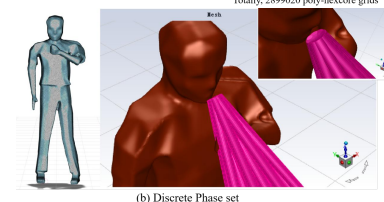
(a) Meshing results

Whole volum mesh
 Fill with: poly-hexcore
 Growth rate: 1.2
 Max cell length [m]: 120

Local sizing
 growth rate: 1.2
 Size control type: face size
 Target mesh size [m]: 5

Whole surface mesh
 Minimum size [m]: 5
 Maximum size [m]: 120
 Growth rate: 1.2
 Size functions: curvature & proximity
 Curvature normal angle: 18
 Cell per gap: 1

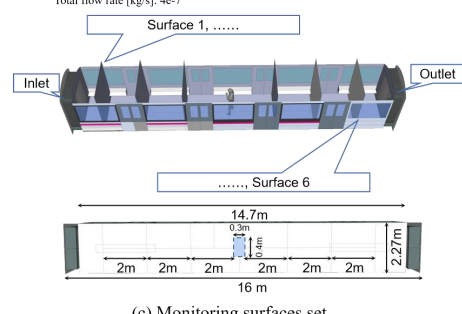
Cabin of 1157895 poly-hexcore grids
 Totally, 2899020 poly-hexcore grids



(b) Discrete Phase set

Material: water-liquid
 Injection geometry: cone
 Diameter distribution: uniform
 Cone type: solid cone
 Number of Streams: 20
 Injection types: 3.5µm, 6µm, 20µm, 50µm, 112µm, 175µm
 Velocity magnitude [m/s]: 21.7
 Cone angle [deg]: 15
 Outer radius [m]: 0.01
 Total flow rate [kg/s]: 4e-7

X-position [m]: 42.199
 Y-position [m]: 10.574
 Z-position [m]: 1.78185
 Period [s]: 0-0.5
 Azimuthal angle [deg]: 360
 X-axis : -0.63304
 Y-axis : 0.00647
 Z-axis : -0.77141



(c) Monitoring surfaces set

Figure 3. The meshing results, the discrete phase set, and monitoring surfaces set of experiments.

2.3 Configurations of CFD simulations

In an attempt to reveal the effect of inertial force on the droplets and the drag force from the airflow. The flow speed will increase due to the drag force in the acceleration phase, while a decrease in the deceleration phase. This could be called the interior induce flow. It is important to note that when the initial direction of droplets jetting is not consistent to the interior

induced flow, what contributes more to the trajectory of different sized droplets.

Firstly, to recognize the temporal and spatial characteristics of interior induced flow, one configuration is constructed: (a) the vacant cabin with the induced flow. The CFD simulation could show how the flow dynamically works during three phases. Secondly, to reveal the effect of inertial force on the droplets and the drag force from the airflow, two configurations are constructed, (b) the manned stationary cabin (inlet facing orientation), and (c) the manned accelerated cabin (inlet facing orientation). In the non-inertial frame, adding the source term to the momentum equation, and setting the inlet boundary conditions, the escape time and X-displacement of various-size droplets have been simulated and analyzed. To compare the trajectory of the droplets under three facing orientations scenes and evaluate the safety distance, this research measures the flux of droplets through six monitoring surfaces, meanwhile simulating and analyzing the escape time and X-displacement of various-size droplets.

- Configuration A: the vacant cabin with the induced flow;
- Configuration B: the manned stationary cabin (inlet facing orientation);
- Configuration C: the manned full-cycle movement cabin (inlet facing orientation);
- Configuration D: the manned accelerated cabin (outlet facing orientation);
- Configuration E: the manned accelerated cabin (side facing orientation);

In a one-station full-cycle period, 0-25s is the acceleration phase; 25-40s is the uniform speed phase; 40-75s is the deceleration phase. The study assumes that the duration of coughing (or sneezing) is assumed to be 0.5 s, with cone injection geometry and a velocity magnitude of 21.7 [m/s]. The dummy model faces toward the inlet, outlet, and the side of the cabin in configurations 3 to 5, respectively. The posture of the dummy model is covering the mouth and nose with the left hand. The particle sizes ejected are divided into six groups: 3.5 μm , 6 μm , 20 μm , 50 μm , 112 μm , 175 μm . The particles are ejected at a 15-degree angle along the circular surface (mouth) at a velocity of 21.7 m/s (Yan et al., 2019) as shown in Figure 2. Since the left arm of the mannequin has a shielding effect, the ejected particles pass through the manikin's hand before floating with the airflow. This transient simulation is calculated in the Ansys benchwork-fluent software (ANSYS), the transient time step is set to 0.02 seconds, and each step is interactively calculated 20 times, from 0s to 75s, a total of 3750 steps. DPM storage results include: particle number, particle diameter, particle mass, time, particle velocity vector, particle displacement in XYZ directions, and tracking particle ID. The six monitoring surfaces are set at 2m, 4m, and 6m on the left and right sides away from the dummy model.

2.4 Infection Probability Index

Although it seems unknown what is the minimum dose of COVID pathogen to cause infection or illness, which is expressed as a function of infection probability (Stadnytskyi et al., 2021), the number of discrete droplets can be counted, over a period of time, through different surface locations using sample trajectories file in the "Discrete phase report" model from the high-fidelity CFD.

In this study, we will deploy the Watanabe dose-response model that has been developed for a variety of airborne infectious diseases including SARS-CoV (Watanabe et al., 2010). In the original model, the probability of infection $P(n)$ is a function of the dose n (Domino, 2020). Therefore, we transform the original infection probability function as:

$$P(n) = 1 - \exp(-n / \text{Ln}(k)), \quad n \in [0, +\infty) \quad (6)$$

where $P(n)$ [%] is an exponential expression of the number of discrete droplet n , the parameter is taken to be $\text{Ln}(k) = -1e+3$ for normalization, which is related to the number of particles tracked. As a conceptual assumption, the inhaled dose is proportional to the total number of droplets.

The $\text{Ln}(k)$ is the most difficult parameter to determine, as it depends on the number of tracked particles. We must take into account the combined effect of dilution of the ambient exhaled air, deposition losses, and pathogen inactivation. It is due to evaporation, convection distance/time from the infectious to the susceptible person, room conditions (RH, temperature, airflow, type of ventilation), anatomical and physiological characteristics of the infectious/susceptible persons, whether or not the infectious person is wearing a face mask (as this significantly affects exhalation flow), and the biological properties of the pathogen. Therefore, it is very difficult, if not impossible, to make a detailed prediction of the situational risk of infection during a one-to-one exposure. Even if one knew an example, the situational variability is so large that exemplary knowledge can hardly be generalized. Thus detailed examples may not help much in guiding infection control measures.

3. RESULTS

3.1 Spatial and Temporal Characteristics of Induced Flow in a Vacant Cabin with Acceleration

The gas is treated as a continuous field when the cabin moves. Talaei et al. (2019) measured and described the spatial and temporal velocity profile of the internal induced flow in the vacant cabin in the duration of acceleration, constant, and deceleration phases. Before the trajectory of droplets is discussed, we firstly simulate and analyze the spatial and temporal characteristics of the cabin-induced airflow. In this study, the spatial and temporal characteristics of the internal airflow organization with the effect of induced flow were dynamically simulated.

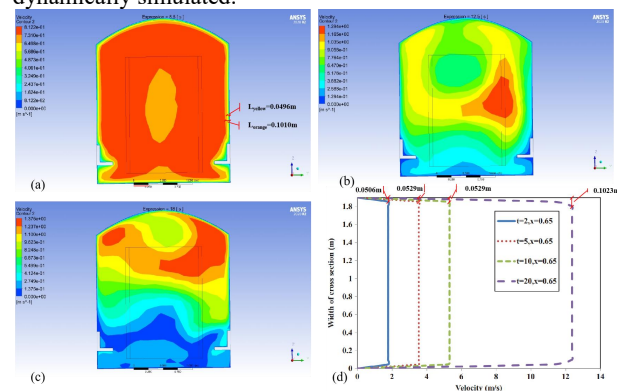


Figure 4. Velocity contour map of interior induced flow in the YZ section. (time-interval is 0.2s)

Figure 1 shows the spatial simulation results of interior induced airflow. According to the cross-sectional flow velocity, the boundary layer always exist in the duration of acceleration and deceleration phases. As shown in Figure 4(a), (b), (c), the thickness of the boundary layer is around 5cm, and the seat geometry forms a low-speed wind area.

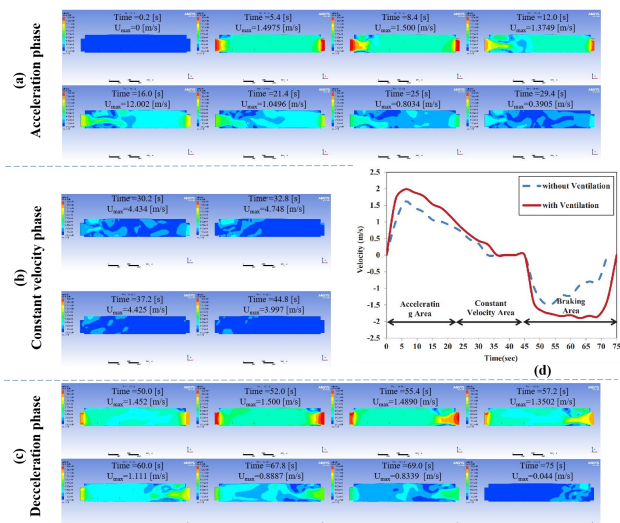


Figure 5. Velocity contour map of interior induced flow in the XZ section. (time-interval is 0.2s but sampling is random)

Figure 5 shows the temporal simulation results of interior-induced airflow. During the acceleration phase, the high-velocity area of airflow is near the inlet of the cabin, while the high-pressure cloud of the air is located at the latter part of the vehicle. The airflow flew into the left entrance and flew out of the right exit. Due to the narrow tube effect, the connecting parts of the cabins on both sides are always high airflow velocity fields. During the deceleration phase, the pattern reversed from before. In the constant stage, there is no relative velocity between the cabin and the internal air, the internal airflow velocity tends to zero, and the air mass pressure distribution is uniform.

3.2 The effects of induced wind and inertial force on the trajectory of droplets

This section aims to explain the induced dragging effect and the inertial effect of the various-size droplets. According to Dbouk et al. (2020), a 2 m distance is safe only when no airflow exists. Blocken et al. (2020) studied the safe distance between two running persons, who are marching in parallel or keeping a fixed distance. Chillón et al. (2021) revealed that while bigger droplets move propelled by inertial and gravitational forces, smaller ones move by the exterior wind environment.

We set up two scenarios, one with background wind and one without wind. In the form of a discrete phase, the droplets ejected by human coughing were set six-size groups: 3.5 μm , 6 μm , 20 μm , 50 μm , 112 μm , 175 μm . The droplets are ejected at a 15-degree angle (Das et al., 2020; Ram et al., 2021) along a circular surface at a velocity of 21.7 m/s and lasting 0.5s). The droplet properties are set to Water-Liquid=1000kg/m³, given a flow rate of 2.4e⁻⁹m³/s, to get the total flow for each droplet size. In Discrete Phase Model, droplets of different sizes are generated; the droplet time step needs to be small enough to meet the tracking requirements: 0.001s; the maximum number of tracked droplets is changed to 50000 to ensure that all ejected droplets are calculated; a solid cone ejection is used to the center of the mouth as the midpoint, and the spray radius is 0.01m; during the period from 0 to 0.5s, 20 strands of each droplet are sprayed.

Under the above condition, it is confirmed that since the position of the left hand of the mannequin is only 12 cm away from the nozzle, the ejected droplets will first pass through the model's hand before escaping with the airflow. In this case, the human body feature is set to the droplet trapped mode, which means absorbing the droplets but not escaping or rebounding.

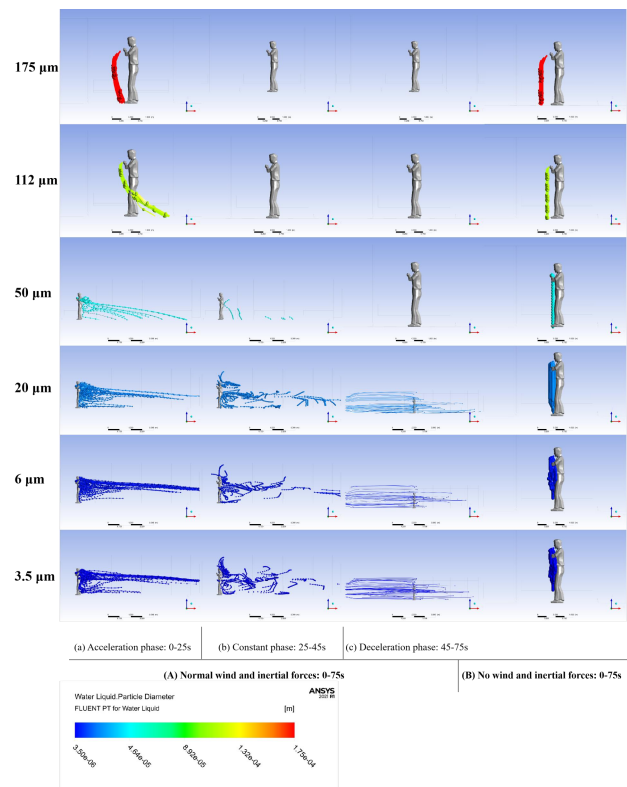
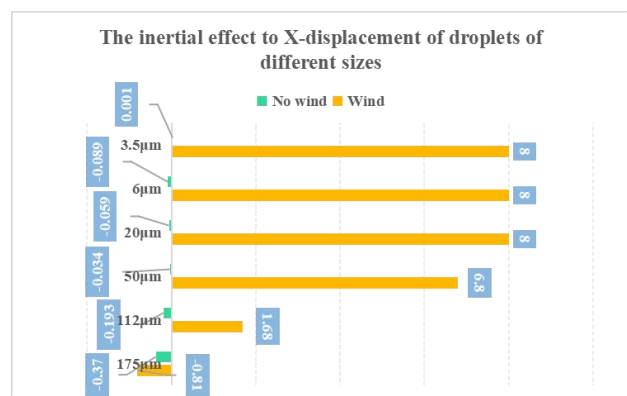


Figure 6. The particle trajectory tracking chart of the normal wind and the no wind configurations. (A) Normal and inertial force effect during 0-75s; (B) No wind effect during 0-75s. (a), (b) and (c) are time-series graphs of six droplet sizes during three phases.

It can be seen from Figure 6 that in the acceleration phase, the induced flow effect significantly affects the trajectory of the droplets, regardless of their large or small sizes. The inertial force effect is mainly manifested on the large-sized droplets, so that they remain in a stable state. In the no background wind configuration, the medium and small-size droplets (20 μm , 6 μm , and 3.5 μm) will suspend in the air around the body within $X = \pm 0.1$ m, and don't flow on the ground.



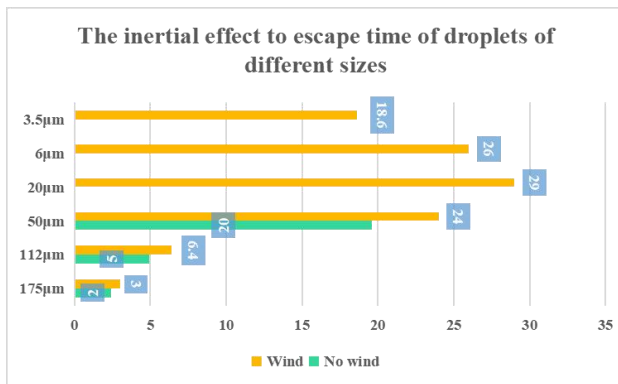


Figure 7. The bar chart of the induced wind and no-wind configurations. (a)X-Displacement and (b)Escape time

Figure 7 illustrates that the moving cabin-induced flow has a significant effect on droplet dispersion, especially for small-size droplets. As reflected from the X-displacement, the impact will cause the droplet to move in the opposite direction, with a maximum distance of 8.059m. From the trap time, the maximum period difference is 29 seconds. The induced wind will prolong the pending duration of droplets. It can be inferred that various mechanical flows will greatly affect the trajectory of droplets, which is more pronounced for small-sized droplets (<50µm).

3.3 The trajectory discrepancy of droplets of three face orientations

Konno et al. (1977) studied the effects of viscous and inertial forces on drop breakup, and found that both the viscous force and the inertial force contribute to the droplet breakup mechanism. Ding and Spelt (2007) studied the effect of droplet spreading, results showed that inertial effects cause droplet spreading to be non-monotonous.

In this study, when an infected person stands inside the moving cabin, the face orientations are the initial velocity directions of droplets. During the three phases of the metro cabin one-station cycle, a droplet is attached with flow drag force and additional acceleration term, so the trajectory of motion will be changed. These values of escape time and X-displacement will suggest to you whether or not to worry about a cough from a passenger whose back is to you.

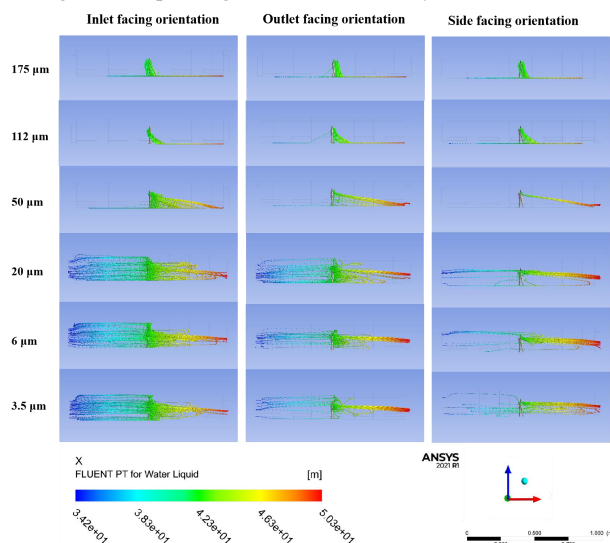


Figure 8. Flow graph of three different facing orientations.

Figure 13 illustrates two points. 1) The motion trend of large-sized (112µm, 175µm) and medium-sized droplets (50µm)

are consistent, and that of the medium-sized and small-sized droplets are consistent (20µm, 6µm, and 3.5µm). The former's trajectory is affected by gravity and inertial force, while the latter is affected by airflow. 2) The face orientations really determine the three-phase motion trajectory of the droplets, if without the cabin-induced airflow or interior mechanical flow. The orientation of the human body only affects the initial state, while the background flow determines not only the movement displacement of the droplets but also the escape time. However, the main determinant is the background flow when it exists. So this convinces us to protect ourselves, whether or not a passenger coughs with his back is to you.

Table 2(a). The escape time of the different-sized droplets (during a one-station cycle, with the Lagrangian tracking droplet model).

Diameters (µm)	Escape time (s)		
	Inlet face orientation	Outlet face orientation	Side face orientation
175	3	3	3
112	6.4	5	5
50	24	17	17
20	29	21.6	21.6
6	26	16.6	17.6
3.5	18.6	16	16.4

Table 2(b). The X-displacement of the different-sized droplets (during a one-station cycle, with the Lagrangian tracking droplet model).

Diameters (µm)	Displacement in X direction (m)		
	Inlet face orientation	Outlet face orientation	Side face orientation
175	-0.81	1.38	0.72
112	1.68	2.7	2.24
50	6.8	7.2	> 8
20	> 8	> 8	> 8
6	> 8	> 8	> 8
3.5	> 8	> 8	> 8

The number of tracked droplets is set to 50000 to ensure that all ejected droplets are calculated; in a period of 0.5s, 20 strands of each droplet were sprayed. Table 2(a) records the fastest escape time (s) of each type of strand; that is, during the time the droplets fall on the boundary wall or escape out of the computational domain. Table 2(b) records the displacement in x-direction (m) of each type of strand; that is, the average displacement in x-direction when the droplets fall on the boundary wall or escape out of the computational domain.

Table 2 illustrates two points. 1) The face orientations differ, and the mean velocity magnitude and turbulence intensity on the leeward side differ. Among three orientations, the side-face position has the high-velocity magnitude, for the body (0.2m*0.4m) blocks the smallest wind shadow area. 2) The droplet sizes differ, the escape time and X displacement differ, and the large-sized droplets are less affected by the induced wind. That explains why the small-sized droplets escape in a shorter time than medium-sized droplets.

3.4 Infection Probability Discrepancy of Six Monitoring Surfaces

Respiratory illnesses can also be spread through the air in tiny, evaporated droplets known as aerosols. When an infected person coughs or sneezes, they shed droplets of saliva, mucus, or other bodily fluids. If any of those droplets fall on you - or if you touch them and then, say, touch your face - you can become infected as well.

This research helps pinpoint the most dangerous places to stand, and shows the level of danger as a certain rainbow color. The project area size of the injector is 0.2*0.4, the distance between the monitoring surfaces and the injector is 2m, 4m, and 6m, and the length of the cabin is 16m.

Passengers' infection probability in different standing positions in contact with an infected person...

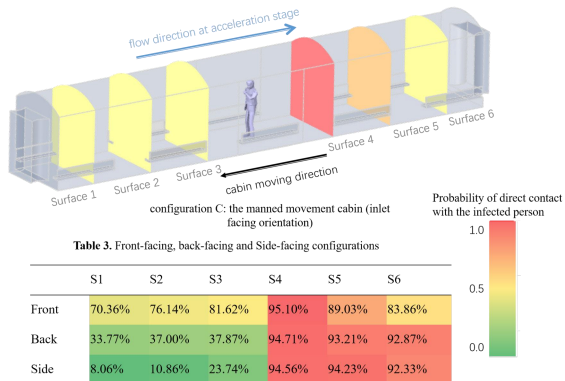


Figure 9. Flow graph of six droplet sizes in three different facing orientations.

From Figure 9, the position that is the most likely to get infectious is at the outlet, regardless of the face orientation. If the probability is set below 30% as a criterion of safety, then only three monitoring positions in the side-facing configuration are safe. This conclusion is unexpected, and conventionally we think that the places behind the infector's back are safe. The reasons are complex. 1) It is mainly because the induced flow in the cabin can change the direction of droplet motion, even the large-size ones. 2) The car-induced flow in the acceleration stage and the deceleration stage are opposite, which leads to an increase in the risk to the whole space in the cabin. A part of the droplets that do not flow out of the cabin in the first stage becomes a later pollution source in the third stage. 3) Considering the wind shadow area size, the human body becomes an obstacle to the spread of droplets, so it slows down the movement of droplets and provides pollution for the reverse movement of droplets in the later stage. Outlet-facing configuration and side-facing configuration could illustrate this point of view.

4. DISCUSSIONS

The innovations of the study are as follows:

- (1) Theoretically, by fully employing two equations regarding the inertial force correction term $F_{inertial}$, the trajectory of sneeze droplets driven by the inertial force and viscous force were simulated under the acceleration straight motion scene.
- (2) In application perspective, few studies that describes the spreading of respiratory viruses in an accelerating cabin were performed. Our study provides an effective way for researching the transmission of the pneumonia virus in metro cabins. Specifically, when the inertial and viscous forces work together on various sizes of droplets, our study highlights the distinctive roles of the induced flow and inertial force on droplets under a acceleration scene.

We note several limitations. In the control experiment, the entire airflow runs through the adjacent cabin, that is, the transfer of the outgoing cabin to the next cabin, fails to be considered. In addition, the difference in the standing and sitting posture of the human body, the influence of the disturbance of the human body motion, and mask screening effect on the airflow are not considered. The evaporation of droplets into dry particles during propagation and the complex problems of

droplet breakup are not considered. These limitations should be addressed in future studies.

In the future, we plan to continue the research in five areas:

(1) This study assumed jet droplets as particles packing up the pathogen, without considering the deformation and evaporation processes. The process of droplets' break-up and evaporation affected by the inertial force will be described in future work.

(2) In order to explore the effect of inertial force, this study did not consider the artificial ventilation mode in the metro cabin in the real scene. In future research, the multiple ventilation modes of top-in, top-out, and top-in, bottom-out will be considered.

(3) The diversity of crowd density and posture effected on droplet spreading exist. In the real scene, passengers in the form of standing, leaning, and sitting postures exist in a common space, and they distribute totally differently. In future research, three levels of sparse, moderate, and dense crowds should be considered, when the droplet dispersion is modeled.

(4) Influence of local airflow uplift and local eddy current caused by human respiration and human body temperature should be considered.

(5) After proving the necessity of the masking strategy, different types of masks, elbow shielding, palm shielding, etc. will be used for testing in the future.

5. CONCLUSIONS

This study investigated the flight trajectories of six-sized droplets driven by drag and inertial forces in the metro cabin-induced wind. For this purpose, the transient problem with time-varying boundary conditions was established and solved and the analytical solutions were calculated. Prior to the simulations, The DPM source terms model was updated into an additional acceleration (force/unit particle mass) term. The function "Vel" was constructed using the "Named Expressions" model. In this context, the non-inertial frame was established and the simulated configurations were as following: 1) spatial and temporal characteristics of induced flow in a vacant cabin with acceleration, 2) the effects of induced wind and inertial force on the trajectory of droplets, 3) the trajectory discrepancy of droplets of three face orientations, and 4) infection probability discrepancy of six monitoring surfaces. The main conclusions drawn from the presented study are as follows:

(1) The induced wind will prolong the pending duration of droplets. It can be inferred that various mechanical flows will greatly affect the trajectory of droplets, which is more pronounced for small-sized droplets (Figure 6, Figure 7).

(2) Among three orientation configurations, the side-face position has the high-velocity magnitude and the smallest wind shadow area. Besides, the droplet sizes differ, the escape time and X displacement differ, and the large-sized droplets are more guided by the inertial force and less affected by the drag force, and vice versa (Figure 8, Table 2).

(3) If the probability is set below 30% as a criterion of safety, then only three monitoring positions in the side-facing configuration are safe. The reasons are complex and worth deeply exploring (Figure 9).

ACKNOWLEDGEMENT

Great assistance from ZRHT Co. Ltd is grateful. They contribute to the technology support of inertial force and viscous force analysis and ANSYS software using. The research study, results of which reported in this manuscript, was partially sponsored by the National Science Foundation

(NSF) under Grants No. 4160010253, the BUCEA foundation of No. ZF15058 and No. X18092, the foundation sponsored by Grants No. H21133. The authors would like to acknowledge and thank the sponsor for this support. Opinions, findings, and conclusions expressed in this manuscript are of the authors and do not necessarily reflect those of the NSF.

REFERENCES

- Aliabadi, A. and Rogak, S., 2011: Langrangian stochastic particle tracking, *Aerosol Science and Technology*, 45, 313-314.
- Blocken, B., Malizia, F., Van Druenen, T., and Marchal, T., 2020: Towards aerodynamically equivalent COVID19 1.5 m social distancing for walking and running, *preprint*.
- Bourouiba, L., 2021: The fluid dynamics of disease transmission, *Annual Review of Fluid Mechanics*, 53, 473-508.
- Bourouiba, L., Dehandschoewercker, E., and Bush, J. W., 2014: Violent expiratory events: on coughing and sneezing, *Journal of Fluid Mechanics*, 745, 537-563.
- Cao, Q., Liu, M., Li, X., Lin, C.-H., Wei, D., Ji, S., Zhang, T. T., and Chen, Q., 2022: Influencing factors in the simulation of airflow and particle transportation in aircraft cabins by CFD, *Building and Environment*, 207, 108413.
- Chillón, S. A., Ugarte-Anero, A., Aramendia, I., Fernandez-Gamiz, U., and Zulueta, E., 2021: Numerical modeling of the spread of cough saliva droplets in a calm confined space, *Mathematics*, 9, 574.
- Das, S. K., Alam, J.-e., Plumari, S., and Greco, V., 2020: Transmission of airborne virus through sneezed and coughed droplets, *Physics of Fluids*, 32, 097102.
- Dbouk, T. and Drikakis, D., 2020: On coughing and airborne droplet transmission to humans, *Physics of Fluids*, 32, 053310.
- Ding, H. and Spelt, P. D., 2007: Inertial effects in droplet spreading: a comparison between diffuse-interface and level-set simulations, *Journal of fluid mechanics*, 576, 287-296.
- Domino, S. P.: Linking High-Fidelity Computational Fluid Dynamics Simulations to Probability of Infection: A Case Study in COVID-19 Transport Deposition Evaporation and Transmission, Sandia National Lab.(SNL-NM), Albuquerque, NM (United States)1061-8562, 2020.
- Doucet, Brian, and Filion, P., 2021: Volume 4: Policy and Planning, Bristol University Press, Project MUSE muse.jhu.edu/book/85126.
- Flügge, G., 1978: Particle spectroscopy.
- Hamidi, S. and Hamidi, I., 2021: Subway ridership, crowding, or population density: determinants of COVID-19 infection rates in New York City, *American journal of preventive medicine*, 60, 614-620.
- Harris, J. E.: The subways seeded the massive coronavirus epidemic in New York City, National Bureau of Economic Research, 2020.
- He, Q., Niu, J., Gao, N., Zhu, T., and Wu, J., 2011: CFD study of exhaled droplet transmission between occupants under different ventilation strategies in a typical office room, *Building and Environment*, 46, 397-408.
- Konno, M., Arai, K., and Saito, S., 1977: The effects of viscous and inertial forces on drop breakup in an agitated tank, *Journal of Chemical Engineering of Japan*, 10, 474-477.
- Li, L.: Study on dust particle distribution in accelerated train, Xi'an University of technology 25-52 pp., 2014.
- Li, X., Lester, D., Rosengarten, G., Aboltins, C., Patel, M., and Cole, I., 2022: A spatiotemporally resolved infection risk model for airborne transmission of COVID-19 variants in indoor spaces, *Science of the Total Environment*, 812, 152592.
- Matsuo, M., Ieda, J. i., Saitoh, E., and Maekawa, S., 2011: Spin-dependent inertial force and spin current in accelerating systems, *Physical Review B*, 84, 104410.
- Mo, B., Feng, K., Shen, Y., Tam, C., Li, D., Yin, Y., and Zhao, J., 2021: Modeling epidemic spreading through public transit using time-varying encounter network, *Transportation Research Part C: Emerging Technologies*, 122, 102893.
- Oleinik, O. A. and Samokhin, V. N., 2018: Mathematical models in boundary layer theory, Routledge
- Palm, M., Allen, J., Liu, B., Zhang, Y., Widener, M., and Farber, S., 2021: Riders who avoided public transit during COVID-19: Personal burdens and implications for social equity, *Journal of the American Planning Association*, 87, 455-469.
- Ram, K., Thakur, R. C., Singh, D. K., Kawamura, K., Shimouchi, A., Sekine, Y., Nishimura, H., Singh, S. K., Pavuluri, C. M., and Singh, R., 2021: Why airborne transmission hasn't been conclusive in case of COVID-19? An atmospheric science perspective, *Science of the Total Environment*, 773, 145525.
- Richmond, J., Isukapalli, S., and Vallero, D., 2011: Air pollutant retention within a complex of urban street canyons, *Atmospheric Environment*, 45, 7612-7618.
- Said, Z., Sundar, L. S., Rezk, H., Nassef, A. M., Ali, H. M., and Sheikholeslami, M., 2021: Optimizing density, dynamic viscosity, thermal conductivity and specific heat of a hybrid nanofluid obtained experimentally via ANFIS-based model and modern optimization, *Journal of Molecular Liquids*, 321, 114287.
- Stadnytskyi, V., Anfinrud, P., and Bax, A., 2021: Breathing, speaking, coughing or sneezing: What drives transmission of SARS-CoV-2?, *Journal of Internal Medicine*, 290, 1010-1027.
- Sun, Y., Bao, E. C., Zhu, C., Yan, L., Cao, Y., Zhang, X., Li, J., Jing, H., and Zou, Z., 2020: Effects of window opening style on inside environment of solar greenhouse based on CFD simulation, *International Journal of Agricultural and Biological Engineering*, 13, 53-59.
- Talaei, M. R., Kabiri, A., Ebrahimi, M., and Hakimzadeh, B., 2019: Analysis of induced interior air flow in subway train cabin due to accelerating and decelerating, *International Journal of Ventilation*, 18, 204-219.
- Wang, T., Tang, C., Chen, R., Ruan, H., Liang, W., Guan, W., Sang, L., Tang, R., Zhong, N., and Li, S., 2020: Clinical features of coronavirus disease 2019 patients with mechanical ventilation: A nationwide study in China, *Critical care medicine*.
- Wang, Y. and Bourouiba, L., 2017: Drop impact on small surfaces: thickness and velocity profiles of the expanding sheet in the air, *Journal of Fluid Mechanics*, 814, 510-534.
- Watanabe, T., Bartrand, T. A., Weir, M. H., Omura, T., and Haas, C. N., 2010: Development of a dose-response model for SARS coronavirus, *Risk Analysis: An International Journal*, 30, 1129-1138.
- Yan, Y., Li, X., and Tu, J., 2019: Thermal effect of human body on cough droplets evaporation and dispersion in an enclosed space, *Building and Environment*, 148, 96-106.
- Yan, Y., Li, X., Yang, L., Yan, P., and Tu, J., 2020: Evaluation of cough-jet effects on the transport characteristics of respiratory-induced contaminants in airline passengers' local environments, *Building and environment*, 183, 107206.
- Yau, Y. H., Chandrasegaran, D., and Badarudin, A., 2011: The ventilation of multiple-bed hospital wards in the tropics: a review, *Building and Environment*, 46, 1125-1132.
- Zeng, D., Zhang, E., Ding, Y., Yi, Y., Xian, Q., Yao, G., Zhu, H., and Shi, T., 2018: Investigation of erosion behaviors of sulfur-particle-laden gas flow in an elbow via a CFD-DEM coupling method, *Powder Technology*, 329, 115-128.
- Zhong, H., Xiong, Q., Zhu, Y., Liang, S., Zhang, J., Niu, B., and Zhang, X., 2019: CFD modeling of the effects of particle shrinkage and intra-particle heat conduction on biomass fast pyrolysis, *Renewable Energy*, 141, 236-245.